Resistive wall modes and nonuniform wall rotation

J. B. Taylor, J. W. Connor, C. G. Gimblett, H. R. Wilson, and R. J. Hastie

Citation: Phys. Plasmas **8**, 4062 (2001); doi: 10.1063/1.1388035
View online: http://dx.doi.org/10.1063/1.1388035
View Table of Contents: http://pop.aip.org/resource/1/PHPAEN/v8/i9
Published by the American Institute of Physics.

Related Articles

Mechanism for magnetic field generation and growth in Rayleigh-Taylor unstable inertial confinement fusion plasmas
Phys. Plasmas 19, 082703 (2012)

Oscillating plasma bubbles. I. Basic properties and instabilities
Phys. Plasmas 19, 082105 (2012)

Kink modes and surface currents associated with vertical displacement events
Phys. Plasmas 19, 082103 (2012)

Internal disruptions and sawtooth like activity in Large Helical Device
Phys. Plasmas 19, 082501 (2012)

Supersonic regime of the Hall-magnetohydrodynamics resistive tearing instability
Phys. Plasmas 19, 072519 (2012)

Additional information on Phys. Plasmas

Journal Homepage: http://pop.aip.org/
Journal Information: http://pop.aip.org/about/about_the_journal
Top downloads: http://pop.aip.org/features/most_downloaded
Information for Authors: http://pop.aip.org/authors

ADVERTISEMENT

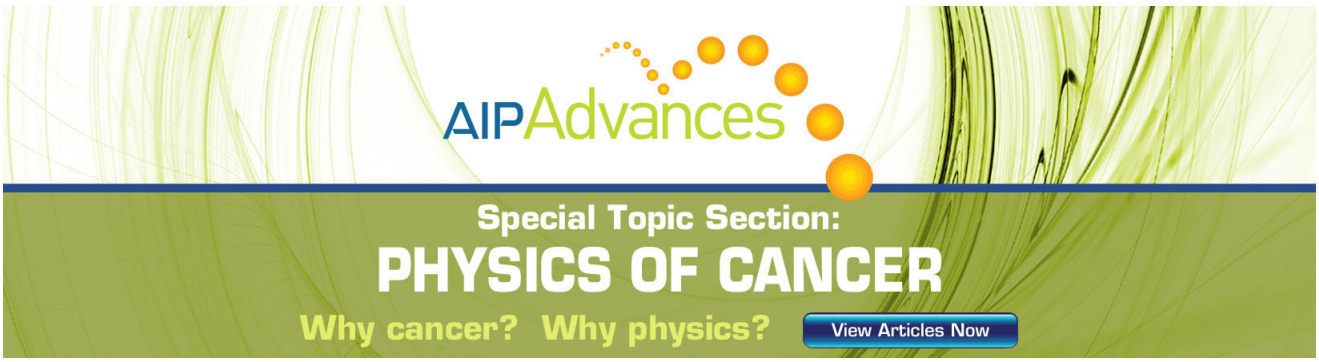

Downloaded 08 Aug 2012 to 194.81.223.66. Redistribution subject to AIP license or copyright; see http://pop.aip.org/about/rights_and_permissions

Resistive wall modes and nonuniform wall rotation

J. B. Taylor, J. W. Connor, C. G. Gimblett, and H. R. Wilson
EURATOM/UKAEA Fusion Association, Culham Science Centre, Abingdon, Oxon OX14 3DB, United Kingdom

R. J. Hastie
MIT Plasma Science & Fusion Center, 167 Albany Street, NW16-234, Cambridge, Massachusetts 02139

(Received 17 April 2001; accepted 5 June 2001)

The resistive wall mode (RWM) poses a threat to many plasma confinement devices. The continuous rotation of the wall relative to the plasma makes it appear perfectly conducting, because of the skin effect, but this is ineffective if the perturbation locks to the wall. This raises the question of whether a nonuniformly rotating wall is more effective. In this paper we discuss the effect of such nonuniform wall rotation, in both the toroidal and poloidal directions, on resonant and nonresonant RWMs. In the case of toroidal rotation it is shown that at large wall velocity both the resonant and nonresonant RWMs are stabilized, even though the nonresonant mode rotates with the maximum wall velocity. In the case of poloidal rotation RWMs do not lock to the wall and have a complicated behavior at intermediate velocities. However they are again stabilized by large wall velocity. © *2001 American Institute of Physics.* [DOI: 10.1063/1.1388035]

I. INTRODUCTION

Resistive wall modes (RWMs) pose a threat to many plasma confinement devices. They are instabilities that arise because the vessel surrounding the plasma is imperfectly conducting. They would not occur if the wall were a perfect conductor, and grow at a rate determined by the vertical field penetration time of the vessel. One of the earliest observations of a RWM was in a Reversed Field Pinch (RFP).[1] In a RFP, the fastest growing RWM is typically nonresonant (i.e., nowhere is the pitch of the perturbation equal to that of the equilibrium magnetic field). This means that the plasma can be considered ideally conducting everywhere. This is also true for the external current-driven kink mode in a tokamak. However, an important RWM in advanced tokamaks is the so-called pressure-driven external kink, which occurs when the plasma exceeds the ''no-wall'' β limit and has been observed in the DIII-D experiment.[2] This mode is essentially toroidal in nature, with the toroidicity and pressure combining to couple neighboring resonant harmonics. It involves nonideal effects at the resonances and must be treated separately.

Bulk rotation of the plasma relative to the wall can result in the plasma ''seeing'' the wall as perfectly conducting, because of the skin effect. However, this stabilizing influence vanishes if the mode ''locks'' to the wall.[3] This has led to the suggestion that there should be a second, rotating wall[4] (possibly simulated by a suitable configuration of external sensors and coils[5]): then the mode cannot simultaneously lock to both walls, and may be stabilized. The proposed use of a flowing lithium wall in a power plant[6] leads to a configuration in which the ''wall'' moves poloidally in opposite directions in the upper and lower halves of the poloidal cross-section. Such nonuniform ''rotation'' should also tend to stabilize the RWM as it cannot lock to the wall everywhere.[7]

In this paper we analyze the effect of nonuniform wall rotation, in both the toroidal and poloidal directions, on RWM stability. A poloidally varying wall rotation couples different poloidal harmonics (labeled by poloidal harmonic number m) of the perturbation and leads to a recurrence relation between them. This relation involves the wall time-constant, the flow velocity and a set of stability indices Δ'_m. These indices depend on the plasma profiles but are independent of rotation. For our present purposes they are considered as given parameters.

For a specific configuration (i.e., given Δ'_m) the problem can readily be solved numerically and we describe some such solutions. However, we first derive some important analytic results that illustrate general features of the problem. These serve to guide and interpret the numerical results. We first investigate the case of toroidal flow $\mathbf{V}=V(\theta)\mathbf{e}_z$, with $\mathbf{e}_z$ a unit toroidal vector and θ the poloidal angle. The basic equation is derived in Sec. II, and the specific case of sinusoidal variation is formulated in Sec. II A. In Sec. II B we investigate the case of small velocity, while in Secs. II C and II D we explore the case of large velocity for nonresonant and resonant modes. This is followed in Secs. II E, II F, and II G by some numerical results, including the critical flow velocity required for stabilization of the (nonresonant) current-driven and (resonant) pressure-driven modes in a tokamak.

We then turn to the case of poloidal flow $\mathbf{V}=V(\theta)\mathbf{e}_\theta$. This problem is formulated in Sec. III and the case of sinusoidal variation is analyzed in Secs. III A, III B, and III C. Numerical results for poloidal flows are presented in Sec. III D, and the special case of a poloidal ''step'' flow with variation $V=V_0\mathrm{sign}(\theta)$ is discussed in Sec. III E. A summary and conclusions are given in Sec. IV.

 © 2001 American Institute of Physics

Downloaded 08 Aug 2012 to 194.81.223.66. Redistribution subject to AIP license or copyright; see http://pop.aip.org/about/rights_and_permissions

II. TOROIDAL FLOWS

The starting point for our investigation is the linearized induction equation for the magnetic perturbation **b** in the wall:

$$\frac{\partial \mathbf{b}}{\partial t} = \nabla \times (\mathbf{V} \times \mathbf{b}) + \eta_W \nabla^2 \mathbf{b}, \tag{1}$$

where η_W is the wall resistivity (assumed uniform). Decomposing the radial component of **b** as

$$b_r = \left(\sum_{m=-\infty}^{\infty} b_m \exp im\theta \right) \exp(pt + ikz), \tag{2}$$

and taking a cylindrical limit, the radial component of Eq. (1) gives

$$\sum_m p b_m \exp im\theta = \sum_m \left(-ikV(\theta) b_m + \eta_W \frac{\partial^2 b_m}{\partial r^2} - \frac{m^2}{r^2} \eta_W b_m \right) \exp im\theta. \tag{3}$$

To connect the interior with the exterior (vacuum) region we integrate Eq. (3) across the wall (radius a, thickness δ_W), to obtain

$$\sum_m (p + ikV(\theta)) \delta_W b_m \exp im\theta = \sum_m (\eta_W / a)(\Delta'_m - m^2 \delta_W / a) b_m \exp im\theta, \tag{4}$$

where Δ'_m is the stability index (at the wall) of the mth poloidal harmonic, namely the dimensionless discontinuity in the logarithmic derivative of b_m across the thin wall:

$$\Delta'_m = \frac{a}{b_m} \left[\frac{db_m}{dr} \right]_{a_-}^{a_+}. \tag{5}$$

Thus, if the wall velocity is

$$V(\theta) = V_0 \sum_n v_n \exp in\theta, \tag{6}$$

then Eq. (4) gives the difference relation

$$p b_m + i \hat{V}_0 \sum_n v_n b_{m-n} = \Delta'_m b_m - \kappa m^2 b_m, \tag{7}$$

where we have introduced the wall time constant $\tau_W = a \delta_W / \eta_W$, normalized p to τ_W, and set $\hat{V}_0 = k V_0 \tau_W$. The dimensionless velocity $\hat{V}_0$ is the key parameter in the problem; the small parameter $\kappa = \delta_W / a$ can help numerical convergence but will be neglected in the analysis that follows.

A. Theoretical analysis—Sinusoidal variation

Now we must choose a functional form for $V(\theta)$. A particularly tractable choice is $V(\theta) = 2V_0 \sin\theta$. Then Eq. (7) reduces to

$$p b_m + \hat{V}_0 (b_{m-1} - b_{m+1}) = \Delta'_m b_m. \tag{8}$$

A useful insight can be obtained by multiplying Eq. (8) by b_m^* and summing over m to find

$$p \sum |b_m|^2 - \sum \Delta'_m |b_m|^2 = \hat{V}_0 \left[\sum (b_m^* b_{m+1} - b_{m+1}^* b_m) \right]. \tag{9}$$

The right-hand side (rhs) of Eq. (9) is purely imaginary, so that

$$\mathcal{R}(p) = \frac{\Sigma \Delta'_m |b_m|^2}{\Sigma |b_m|^2} \tag{10}$$

[a similar result applies for any anti-symmetric $V(\theta)$]. This identity illustrates how differential rotation can lead to stabilization, even though $\hat{V}_0$ does not appear explicitly in it. At $\hat{V}_0 = 0$ an unstable RWM is associated with a single positive Δ'_m; indeed $\mathcal{R}(p) = \Delta'_m$.[3] As $\hat{V}_0$ increases, the coupling between the b_m given by Eq. (8) will cause the b_m spectrum to broaden so that $\mathcal{R}(p)$ is influenced by other Δ'_m. At high m these are vacuum-like with $\Delta'_m \sim -2|m|$, so that the growth rate is reduced below its zero velocity value.

Another feature of Eq. (8) is that when we reverse the direction of the flow, $\hat{V}_0 \to -\hat{V}_0$, the Fourier modes $b_m \to b_m \exp im\pi$, so that if the original b_m were of the same sign, those for reversed flow would alternate in sign. However, this phase change has no effect on the growth rate.

B. Small velocity

We first analyze Eq. (8) for the case of small $\hat{V}_0$. Starting from the $\hat{V}_0 = 0$ solution, when only one b_m is excited and $p_m = \Delta'_m$, the first order perturbation vanishes (in agreement with the fact that $\hat{V}_0 \to -\hat{V}_0$ has no effect on mode frequency). By iterating Eq. (8) we find

$$(p_m - \Delta'_m) b_m = \hat{V}_0^2 \left[\frac{b_{m+2} - b_m}{p_m - \Delta'_{m+1}} - \frac{b_m - b_{m-2}}{p_m - \Delta'_{m-1}} \right], \tag{11}$$

so to $\mathcal{O}(\hat{V}_0)^2$,

$$(p_m - \Delta'_m) + \hat{V}_0^2 \left[\frac{1}{\Delta'_m - \Delta'_{m+1}} + \frac{1}{\Delta'_m - \Delta'_{m-1}} \right] = 0. \tag{12}$$

If m now refers to the most unstable RWM at $\hat{V}_0 = 0$, we have

$$\Delta'_m > \Delta'_{m+1}, \Delta'_{m-1}, \tag{13}$$

so that

$$p_m \sim \Delta'_m - \mu \hat{V}_0^2, \tag{14}$$

where μ is positive. Hence, as expected, $\hat{V}_0$ reduces the growth of the most unstable RWM. In the case of the second most unstable mode, the inequalities (13) are replaced by

$$\Delta'_{m+1} > \Delta'_m > \Delta'_{m-1}, \tag{15}$$

and μ can be of either sign, depending on the relative values of the three largest Δ's.

Downloaded 08 Aug 2012 to 194.81.223.66. Redistribution subject to AIP license or copyright; see http://pop.aip.org/about/rights_and_permissions

C. Large velocity, nonresonant modes

We now turn to the case of large rotational velocity $\hat{V}_0$, where we expect a broad spectrum of b_m to be excited. We write $b_m = \exp i\phi_m$ so that the difference equation (8) becomes

$$(p-\Delta'_m) = \hat{V}_0[\exp i(\phi_{m+1}-\phi_m) - \exp i(\phi_{m-1}-\phi_m)]. \tag{16}$$

This suggests that either p or some Δ'_m becomes large as $\hat{V}_0 \to \infty$. Only the former can occur for nonresonant modes and in this case we put $p = 2i\hat{V}_0 \sin\alpha$. Then, treating m as a continuous variable and assuming that $d\phi/dm$ varies slowly, we have

$$\sin\left(\frac{d\phi(m)}{dm}\right) = \sin\alpha + \frac{i\Delta'_m}{2\hat{V}_0}, \tag{17}$$

so that

$$\frac{d\phi}{dm} = \alpha + g, \quad \text{or} \quad \pi - (\alpha+g), \tag{18}$$

where $g \to 0$ as $\hat{V}_0 \to \infty$. If $\alpha \neq \pi/2$,

$$g \simeq \frac{i\Delta'_m}{2\hat{V}_0 \cos\alpha}, \tag{19}$$

and if $\alpha = \pi/2$,

$$g \simeq \pm(i-1)\sqrt{\frac{|\Delta'_m|}{2\hat{V}_0}}. \tag{20}$$

For definiteness we choose the root such that $\mathcal{I}(g) < 0$ as $|m| \to \infty$. Then the appropriate forms for b_m are the right solution ($b_m \to 0$ as $m \to +\infty$),

$$b_m \simeq \exp i\left((\pi-\alpha)m - \int^m g\,dm\right), \tag{21}$$

and the left solution ($b_m \to 0$ as $m \to -\infty$),

$$b_m \simeq \exp i\left(\alpha m + \int^m g\,dm\right). \tag{22}$$

These solutions are valid for all m as $\hat{V}_0 \to \infty$, but must be matched at an intermediate m. To do this we return to the exact difference equation,

$$2i\sin\alpha - \frac{\Delta'_m}{\hat{V}_0} = \left(\frac{b_{m+1}}{b_m} - \frac{b_{m-1}}{b_m}\right). \tag{23}$$

Then, for large $\hat{V}_0$, from Eqs. (21), (22) and (23), we have

$$2i\sin\alpha \simeq -2\exp(-i\alpha), \tag{24}$$

so that $\alpha = \pm\pi/2$. The mode frequency is therefore

$$p = \pm 2i\hat{V}_0, \tag{25}$$

and the phase change between adjacent Fourier harmonics is $\pi/2$ for both positive and negative m. (Note that these results are independent of which m we choose for matching the left and right solutions.)

An estimate of the damping $\mathcal{R}(p)$ of this mode can be obtained from the identity derived earlier, Eq. (10),

$$\mathcal{R}(p) = \frac{\Sigma\Delta'_m|b_m|^2}{\Sigma|b_m|^2}. \tag{26}$$

From Eqs. (20), (21) and (22) the spectrum at large m is

$$|b_m|^2 \simeq \exp\left(-\frac{4}{3}\frac{|m|^{3/2}}{\hat{V}_0^{1/2}}\right), \tag{27}$$

which extends to $|m| \sim \hat{V}_0^{1/3}$. Consequently at large $\hat{V}_0$, $\mathcal{R}(p)$ becomes independent of the spectrum at small $|m|$ and, replacing sums by integrals, tends to

$$\mathcal{R}(p) \simeq \frac{-\int_0^\infty 2m\exp(-4m^{3/2}/3\hat{V}_0^{1/2})dm}{\int_0^\infty \exp(-4m^{3/2}/3\hat{V}_0^{1/2})dm}, \tag{28}$$

i.e.,

$$\mathcal{R}(p) \simeq -\frac{(9\hat{V}_0/2)^{1/3}\Gamma(4/3)}{\Gamma(2/3)} \simeq -1.09\hat{V}_0^{1/3}. \tag{29}$$

Finally, therefore, at large $\hat{V}_0$,

$$p \simeq \pm 2i\hat{V}_0 - 1.09\hat{V}_0^{1/3}. \tag{30}$$

Physically this solution corresponds to a stable mode that travels toroidally at the maximum wall speed [presumably because mode locking is most effective where $V(\theta)$ is stationary in θ]. The frequency, damping and structure of this mode do not depend on Δ'_m; consequently it is a *universal* mode, independent of low $|m|$ features and therefore of the plasma profile!

D. Large velocity, resonant modes

In advanced tokamaks a performance limiting instability is the RWM that arises from the pressure-driven external kink.[2] The mode is essentially toroidal, with resonant sidebands driven by toroidicity and β. This does not lend itself readily to analytic investigation. However, a cylindrical model of this mode can be constructed, as demonstrated by Finn,[8] who modeled the toroidal mode by a cylindrical equilibrium that was ideal unstable in the absence of a wall, but had a resonance in the plasma at $r = r_s$. It was shown in Refs. 9 and 10 that this construction leads to the relation

$$\Delta'_2(r_s) = \left(\frac{1-\delta\Delta'_2(r_W)}{\Delta'_2(r_W)-\epsilon}\right), \tag{31}$$

between the *plasma* response at the resonant layer, $\Delta'_2(r_s)$, and the *wall* response $\Delta'_2(r_W)$. (The subscript 2 indicates that we are taking the internal plasma resonance to be associated with $m=2$.) The parameter $\epsilon > 0$ represents the degree of ideal instability in the absence of a wall, $\Delta'_2(r_W) \to 0$, and $\delta > 0$ represents the degree of tearing stability in the presence of an ideal wall, $\Delta'_2(r_W) \to \infty$.

With this qualitative model, the resonant RWM can be investigated by solving Eq. (31) for the wall response $\Delta'_2(r_W)$ when the plasma resonant layer response $\Delta'_2(r_s)$ is given. We take this layer response to be the ''visco-resistive''

Downloaded 08 Aug 2012 to 194.81.223.66. Redistribution subject to AIP license or copyright; see http://pop.aip.org/about/rights_and_permissions

form $\Delta_2'(r_s)=p\tau_V/\tau_W$ (where τ_V is a hybrid layer time) believed to be relevant for many tokamaks.[11] For simplicity we also take $\tau_V=\tau_W$. Finally, then, we have for the Δ_2' to be used in Eq. (8):

$$\Delta_2'=\left(\frac{1+\epsilon p}{\delta+p}\right). \tag{32}$$

Note that, unlike the earlier discussion, Δ_2' now explicitly depends on p.

The effect of differential wall rotation on resonant RWMs is quite different from the effect in the nonresonant case. This is because the resonant $\Delta_2'\to\infty$ as $p\to-\delta$. This leads to a narrow spectrum of b_m despite the coupling introduced by wall rotation.

Returning to Eq. (17) we have

$$\sin\left(\frac{d\phi}{dm}\right)=\frac{1}{2i\hat{V}_0}(p-\Delta_m'), \tag{33}$$

so at large $\hat{V}_0$, for all Δ_m' except $m=2$,

$$\frac{d\phi}{dm}=\frac{1}{2i\hat{V}_0}(p-\Delta_m') \quad \text{or} \quad \pi-\frac{1}{2i\hat{V}_0}(p-\Delta_m'). \tag{34}$$

Therefore, for $m<2$,

$$b_m\simeq\exp\left[\frac{1}{2\hat{V}_0}\left(mp-\int^m\Delta_m'dm\right)\right], \tag{35}$$

and for $m>2$,

$$b_m\simeq\exp\left[i\pi m-\frac{1}{2\hat{V}_0}\left(mp-\int^m\Delta_m'dm\right)\right]. \tag{36}$$

As before, we have to match these two solutions, but now we *must* do so at $m=2$. As $\hat{V}_0\to\infty$, Eq. (35) gives $b_{m+1}/b_m\to-1$ for $m<2$ and Eq. (36) gives $b_{m-1}/b_m\to+1$ for $m>2$, so matching these at $m=2$ leads to the dispersion relation

$$(p-\Delta_2')=-2\hat{V}_0, \tag{37}$$

i.e.,

$$\left(p-\frac{1+\epsilon p}{\delta+p}\right)=-2\hat{V}_0. \tag{38}$$

Therefore, as expected, when $\hat{V}_0\to\infty$, $p\to-\delta$. We are only interested in RWMs if the system would be stable with an ideal wall, i.e., if $\delta>0$, hence in cases of interest the resonant RWM is stable at large wall velocity. (Essentially this stabilization comes about because in this case the skin effect really does make the wall appear ideal.) The Fourier spectrum is peaked at $m=2$ and for $m<2$ adjacent harmonics b_m have the same phase, whereas for $m>2$ they have opposite phase. As remarked earlier, this behavior is reversed if $\hat{V}_0\to-\hat{V}_0$. Note that this resonant mode does *not* lock to the wall and that it is again universal, in the sense that it is independent of all Δ_m' except the resonant Δ_m'.

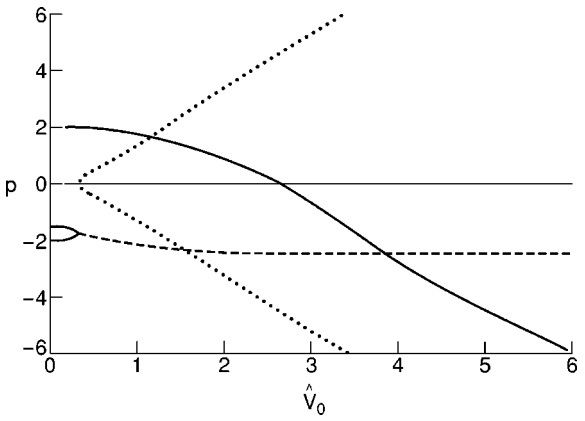

FIG. 1. The effect of a toroidal $\sin\theta$-dependent flow on a nonresonant RWM. (i) Solid line, real eigenvalue p. (ii) Broken line, Re(p). (iii) Dotted line, Im(p).

E. Numerical solution of the toroidal flow case

Equation (8) was solved numerically both by matrix inversion and using a ''shooting'' method. A model is needed for the set of Δ_m' values. Of course, for a specific situation one would determine the equilibrium profile and numerically calculate these quantities. However, for an initial investigation this is not necessary, and we can assign them plausible values. The unstable nonresonant RWM was chosen to be $m=3$ and represented by setting Δ_3' to $+2$. In a cylindrical model the $\Delta_{\pm1}'$ are universal (due to the ''top hat'' nature of the eigenfunction) and for all equilibria,

$$\Delta_{\pm1}'=\frac{-2q_a}{q_a\mp1}, \tag{39}$$

where q_a is the wall value of the safety factor which we take to be $q_a=3$. The remaining Δ_m' were set to the vacuum response, i.e., $\Delta_0'=-2$, $\Delta_m'=-2|m|$.

F. Nonresonant modes

The results of a typical numerical calculation are shown in Fig. 1. (In all figures the solid lines denote a purely real eigenvalue p and the broken and dotted lines denote the real and imaginary parts of a complex eigenvalue.) It can be seen that the growth rate of the most unstable RWM ($p=2$ at $\hat{V}_0=0$) decreases with velocity, in fact in close agreement with Eq. (14). For this mode the eigenvalue p remains real (i.e., the mode does not spin up or lock to the wall) and it becomes stable at $\hat{V}_0\simeq2.6$.

Figure 1 also shows two other modes, which are stable at $\hat{V}_0=0$. These coalesce at $\hat{V}_0\simeq0.33$ and begin to ''spin up,'' as indicated by complex p, eventually approaching the maximum wall velocity [$\mathrm{Im}(p)\sim2i\hat{V}_0$, in accord with Eq. (30)]. Note that this mode has the smallest damping rate for $\hat{V}_0\gtrsim3.9$, i.e., at large $\hat{V}_0$ the least damped mode *is* the universal nonresonant mode described in Sec. II C.

Downloaded 08 Aug 2012 to 194.81.223.66. Redistribution subject to AIP license or copyright; see http://pop.aip.org/about/rights_and_permissions

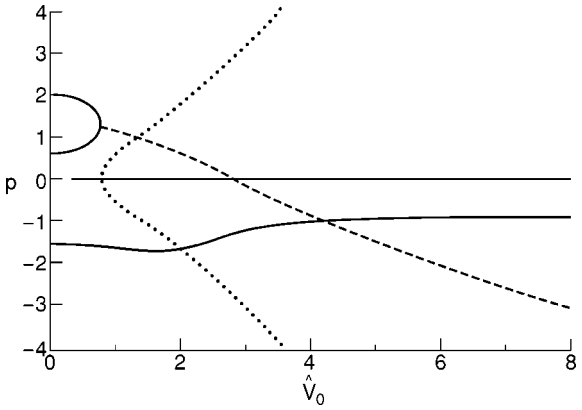

FIG. 2. The effect of a toroidal sin θ-dependent flow on a resonant RWM. (i) Solid line, real eigenvalue p. (ii) Broken line, Re(p). (iii) Dotted line, Im(p).

G. Resonant modes

As mentioned earlier, an important mode in a tokamak is the pressure-driven external kink RWM, which is essentially toroidal and involves a resonant plasma layer. In Sec. II D we described a simple cylindrical model that mimics this toroidal mode and leads to the form for $\Delta_2'(r_W)$,

$$\Delta_2' = \left(\frac{1+\epsilon p}{\delta + p} \right). \tag{40}$$

For numerical work we take $\epsilon = 0.1$ and $\delta = 1.0$, keeping other parameters as in the nonresonant calculation. The results are shown in Fig. 2. At $\hat{V}_0 = 0$ there is an unstable $m = 3$ RWM with $p = 2$, and an unstable $m = 2$ mode with $p \simeq 0.6$, arising from Eq. (40). We see that as $\hat{V}_0$ increases these two modes coalesce (at $\hat{V}_0 \simeq 0.8$) to give modes with complex eigenvalues. These are eventually stabilized at $\hat{V}_0 \sim 2.8$. There is also a stable $m = 2$ mode, with $p \sim -1.6$ at $\hat{V}_0 = 0$. For this mode p remains real as $\hat{V}_0$ increases and for $\hat{V}_0 \gtrsim 4$ it becomes the least damped mode. Its eigenvalue asymptotes to $p = -\delta$ in accord with the analysis in Sec. II D.

III. POLOIDAL FLOWS

The starting point for the analysis of the effect of poloidal wall rotation is again Eq. (1) where the flow is now $\mathbf{V} = V(\theta)\mathbf{e}_\theta$. For a general poloidal flow,

$$V(\theta) = V_0 \sum v_n \exp in\theta, \tag{41}$$

we obtain

$$p b_m + im\hat{V}_0 \sum_n v_n b_{m-n} = \Delta_m' b_m, \tag{42}$$

where now $\hat{V}_0 = V_0 \tau_W / a$. Note that the toroidal wave number does not appear explicitly in Eq. (42). As noted earlier, a flowing lithium blanket could be modeled as a counter rotating flow in upper and lower halves of the poloidal cross-section ["step flow" $V = V_0 \,\mathrm{sign}(\theta)$]. This would correspond to coefficients

$$\begin{aligned} v_n &= -\frac{2i}{\pi n}, \quad n \ \text{odd}, \\ &= 0, \quad n \ \text{even}, \end{aligned} \tag{43}$$

and introduces coupling between all Fourier harmonics b_m, as well as requiring singularities at $\theta = 0, \pi$. Accordingly, we consider first the much simpler case of sinusoidal variation $V = -2\hat{V}_0 \sin\theta$ (which could be approximately realized by a blanket fed by a suitable array of injection and extraction points around the periphery of the tokamak).

A. Analysis of poloidal flows—a "standard model"

For a poloidal flow with a sinusoidal variation, Eq. (42) reduces to

$$(p - \Delta_m') b_m + m\hat{V}_0 (b_{m+1} - b_{m-1}) = 0. \tag{44}$$

Although this is similar to the equation for toroidal flow [Eq. (8)], the two cases are significantly different. With toroidal flow the wall velocity is constant along the direction of motion, whereas with poloidal flow the wall velocity changes, and indeed reverses, along the direction of motion. Consequently we expect "wall locking" to be more strongly inhibited with poloidal flows.

A remarkable feature of Eq. (44) is that positive and negative harmonics (m-numbers) are decoupled from each other, and $b_0 = 0$ except for the $m = 0$ mode (which is unaffected by rotation). By exploiting these features we can obtain an *exact* solution for a particular set of Δ_m'. This special solution then forms the basis for some important general results.

The exact solution is obtained by taking $\Delta_m' = -2|m|$ for all m. Then

$$(p + 2m) b_m + m\hat{V}_0 (b_{m+1} - b_{m-1}) = 0. \tag{45}$$

Multiplying this by $\exp im\theta$, and summing over positive m gives

$$\left(p - 2i \frac{\partial}{\partial \theta} \right) b(\theta) - 2\hat{V}_0 \frac{\partial}{\partial \theta} (b(\theta) \sin\theta) = 0, \tag{46}$$

where $b(\theta) = \Sigma b_m \exp im\theta$. Then

$$b(\theta) = \frac{1}{(1 - i\hat{V}_0 \sin\theta)} \exp\left\{ -\frac{ip}{2} \int^\theta \frac{d\theta}{(1 - i\hat{V}_0 \sin\theta)} \right\}. \tag{47}$$

Since $b(\theta)$ must be periodic, we obtain the exact eigenvalue,

$$p = -2m(1 + \hat{V}_0^2)^{1/2}: \quad m = \text{positive integer}, \tag{48}$$

with the corresponding eigenfunction

$$b(\theta) = \frac{1}{(1 - i\hat{V}_0 \sin\theta)} \left\{ \frac{\tan\theta/2 - i\hat{V}_0 - i(1 + \hat{V}_0^2)^{1/2}}{\tan\theta/2 - i\hat{V}_0 + i(1 + \hat{V}_0^2)^{1/2}} \right\}^m. \tag{49}$$

We see that for this "standard model," all RWMs are stable and the damping rate increases with the wall velocity, asymptotically approaching $-2m\hat{V}_0$. All eigenvalues are purely real so that, as expected, there is no "wall locking."

Downloaded 08 Aug 2012 to 194.81.223.66. Redistribution subject to AIP license or copyright; see http://pop.aip.org/about/rights_and_permissions

Although this model ($\Delta'_m=-2|m|$) is valuable as a benchmark for numerical computations it is clearly not representative of more general situations—particularly as in it all RWMs are stable for any wall velocity! However, this restricted model forms the basis for an important extension to RWMs with arbitrary values of Δ'_m and large wall velocity.

B. Analysis of poloidal flows—a general large *V* model

The basis for extending the restricted model to more general cases is the following observation. If we introduce $\hat{p}=p/\hat{V}_0$ the fundamental equation becomes

$$\left(\hat{p}-\frac{\Delta'_m}{\hat{V}_0}\right)b_m+m(b_{m+1}-b_{m-1})=0. \tag{50}$$

This suggests that at large $\hat{V}_0,\Delta'_m$ is unimportant unless it is itself large. However, except for the resonant mode, Δ'_m is large only at large m—where it always has the standard value $-2|m|$. Accordingly we expect that, irrespective of the Δ'_m for small m (i.e., irrespective of the plasma profile) the eigenvalues of Eq. (50) will always tend asymptotically to those of the standard model as $\hat{V}_0$ increases. This is demonstrated for a single nonstandard Δ'_m, in detail below.

Consider a model in which only one Δ'_m differs from the standard value, i.e., $\Delta'_m=-2|m|$ for $m\neq l$ and Δ'_l is arbitrary. Then, if we carry out the same steps as in solving the standard model, we obtain in place of Eq. (46),

$$2\frac{\partial}{\partial\theta}(\hat{V}_0\sin\theta+i)b(\theta)-pb(\theta)$$
$$=-(\Delta'_l+2l)\exp il\theta\oint\frac{d\theta}{2\pi}b(\theta)\exp(-il\theta). \tag{51}$$

Putting $(\hat{V}_0\sin\theta+i)=r(\theta)$, $r(\theta)b(\theta)=h(\theta)$ and

$$\oint\frac{d\theta}{2\pi}\frac{h(\theta)}{r(\theta)}\exp(-il\theta)=H, \tag{52}$$

Eq. (51) can be written as

$$\frac{\partial h}{\partial\theta}-\frac{p}{2}\frac{h(\theta)}{r(\theta)}=-\frac{(\Delta'_l+2l)}{2}\exp(il\theta)H. \tag{53}$$

Therefore

$$h(\theta)\exp\left(-\frac{p}{2}R(\theta)\right)$$
$$=-\left[\frac{(\Delta'_l+2l)}{2}\int_{-\pi}^{\theta}\exp\left(-\frac{p}{2}R(\theta')+il\theta'\right)d\theta'\right]H+1, \tag{54}$$

where

$$R(\theta)=\int_0^{\theta}\frac{d\theta'}{r(\theta')}, \tag{55}$$

and h is normalized so that the integration constant is unity.

Introducing

$$I_1=\oint\exp\left(-\frac{p}{2}R(\theta)+il\theta\right)d\theta,$$

$$I_2=\frac{1}{2\pi}\oint\exp\left(\frac{p}{2}R(\theta)-il\theta\right)\frac{d\theta}{r(\theta)},$$

and

$$I_3=\frac{1}{2\pi}\oint\frac{1}{r(\theta)}\exp\left(\frac{p}{2}R(\theta)-il\theta\right)d\theta$$
$$\times\int_{-\pi}^{\theta}\exp\left(-\frac{p}{2}R(\theta')+il\theta'\right)d\theta', \tag{56}$$

Eqs. (52) and (54) give

$$\left[1+\frac{(\Delta'_l+2l)}{2}I_3\right]H=I_2. \tag{57}$$

Since $h(\theta)$ must be periodic, Eq. (54) also gives

$$\exp\left[-\frac{p}{2}R(2\pi)\right]-1=-\frac{(\Delta'_l+2l)}{2}I_1H, \tag{58}$$

i.e.,

$$\exp\left(\frac{ip\pi}{(1+\hat{V}_0^2)^{1/2}}\right)-1=\frac{-(\Delta'_l+2l)I_1I_2}{(2+(\Delta'_l+2l)I_3)}. \tag{59}$$

This equation gives the RWM frequency p in a form that involves only standard integrals. Its immediate importance is that it can be shown (see the Appendix) that the expression on the right hand side of Eq. (59) tends to zero as $\hat{V}_0\to\infty$. Thus, irrespective of Δ'_l the eigenvalues p approach those of the standard model as the rotation speed increases.

C. Marginal stability and $p=0$

An indication of the complicated behavior of RWMs in the intermediate region between small rotation velocity (where $p_m\sim\Delta'_m$) and large rotation velocity [where $p_m\to-2m(1+\hat{V}_0^2)^{1/2}$] can be obtained by examining the case $p=0$. We consider a model in which a few, small m, parameters Δ'_m, may be arbitrary and the remainder have their standard values $-2|m|$ (i.e., $\Delta'_m=-2|m|$ for $m\geqslant m_0$). (This is the typical situation for model tokamak plasmas.) Then, for $p=0$ and $m\geqslant m_0$,

$$2b_m+\hat{V}_0(b_{m+1}-b_{m-1})=0, \tag{60}$$

so that $b_m=\lambda^m$ with

$$\lambda=\left(1+\frac{1}{\hat{V}_0^2}\right)^{1/2}-\frac{1}{\hat{V}_0}. \tag{61}$$

(For $\hat{V}_0>0$, $\lambda<1$ so that $b_m\to0$ as $m\to\infty$.) We now match this solution to that obtained by repeated application of the difference equation,

$$-\frac{\Delta'_m}{m}b_m+\hat{V}_0(b_{m+1}-b_{m-1})=0, \tag{62}$$

Downloaded 08 Aug 2012 to 194.81.223.66. Redistribution subject to AIP license or copyright; see http://pop.aip.org/about/rights_and_permissions

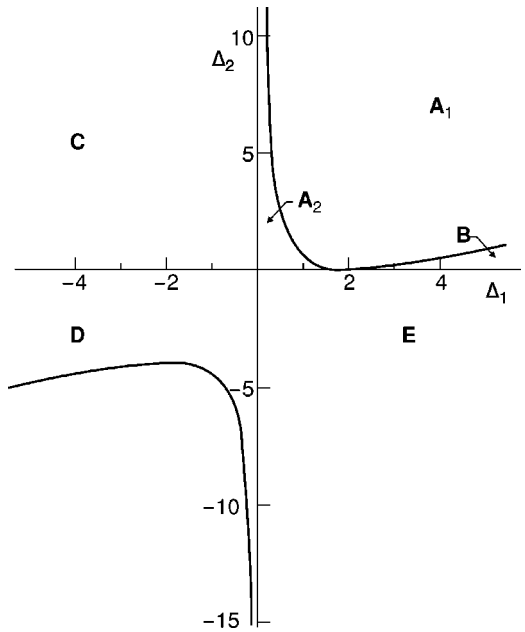

FIG. 3. The different regimes for two nonstandard Δ's.

starting from $b_0=0$. For example, in the simplest case that only Δ_1' differs from its standard value, we use Eq. (62) to obtain b_2/b_1 and match it to $b_m=\lambda^m$, i.e.,

$$\frac{\Delta_1'}{\hat{V}_0}=\frac{b_2}{b_1}=\lambda=\left(1+\frac{1}{\hat{V}_0^2}\right)^{1/2}-\frac{1}{\hat{V}_0}. \tag{63}$$

Thus, if $\Delta_1'>0$, the critical velocity $\hat{V}_c$ at which $p=0$ is

$$\hat{V}_c^2=(1+\Delta_1')^2-1. \tag{64}$$

This is in accord with the fact that there is a single unstable mode at $\hat{V}_0=0$ that becomes stable at $\hat{V}_0=\hat{V}_c$, and $\hat{V}_c$ is the true stability boundary. (If $\Delta_1'<0$ there is no real velocity for which $p=0$ as all modes are stable for all $\hat{V}_0$.)

The situation is more complicated when more than one Δ_m' differs from its standard value. For example, when Δ_1' and Δ_2' are nonstandard we have, for $m=1$,

$$\frac{\Delta_1'}{\hat{V}_0}=\frac{b_2}{b_1}, \tag{65}$$

and for $m=2$,

$$\frac{\Delta_2'}{2\hat{V}_0}=\frac{b_3}{b_2}-\frac{b_1}{b_2}, \tag{66}$$

so that matching b_3/b_2 to $b_m=\lambda^m$ gives for the critical velocity

$$\frac{\Delta_2'}{2}+\frac{\hat{V}_0^2}{\Delta_1'}=(1+\hat{V}_0^2)^{1/2}-1. \tag{67}$$

As a function of Δ_1',Δ_2' there are now several distinct regimes, as shown in Fig. 3.

(a) If $\Delta_1'<0$, $\Delta_2'<0$ (Region D), Eq. (67) has no valid roots. This is in accord with the fact that all RWMs are stable for any velocity, so there is no marginal stability boundary.

(b) If $\Delta_1'<0$, $\Delta_2'>0$, or $\Delta_1'>0$, $\Delta_2'<0$ (Regions C,E), Eq. (67) has one valid root. In this region there is one stable and one unstable eigenvalue at $\hat{V}_0=0$. However, as we will see in Sec. III D, the point $p=0$ need not correspond to the unstable eigenvalue becoming stable. Instead it may correspond to the stable one becoming unstable! Consequently $p=0$ is not necessarily the marginal stability boundary in this regime.

(c) If $\Delta_1'>0$, $\Delta_2'>0$, there are three subregions to consider.

(i) In region A_1, with $\Delta_2'>f(\Delta_1')$ where
$$f(\Delta_1')=\frac{(\Delta_1'-2)^2}{2\Delta_1'}, \tag{68}$$
and region A_2 with $\Delta_2'<f(\Delta_1')$ and $\Delta_1'<2$, Eq. (67) has no valid roots. This is despite the fact that there are two unstable eigenvalues at $\hat{V}_0=0$ that become stable as $\hat{V}_0\to\infty$. This is an indication that the eigenvalues become complex before stabilization.

(ii) In region B, with $\Delta_2'<f(\Delta_1')$ and $\Delta_1'>2$, Eq. (67) has two real roots. In this case the larger root may represent the marginal stability boundary but, as in (b) above, this is not always the case.

We now examine the behavior in each of these regions in detail.

D. Numerical solution with poloidal flow

We have investigated each of the distinct regions identified in the previous section by numerical computation, again using matrix inversion and a shooting code. In both methods, particularly at high $\hat{V}_0$, great care must be taken to retain an appropriate number of b_m. A summary of the results is as follows.

(a) In region D ($\Delta_1'<0,\Delta_2'<0$) all modes are stable at all velocities. There are two typical ways in which the

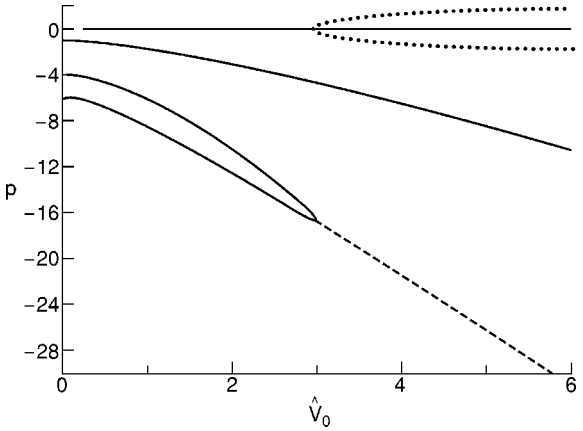

FIG. 4. The effect of poloidal $\sin\theta$-dependent flow, $\Delta_1'=-1.0$, $\Delta_2'=-4.0$. (i) Solid line, real eigenvalue p. (ii) Broken line, Re(p). (iii) Dotted line, Im(p).

Downloaded 08 Aug 2012 to 194.81.223.66. Redistribution subject to AIP license or copyright; see http://pop.aip.org/about/rights_and_permissions

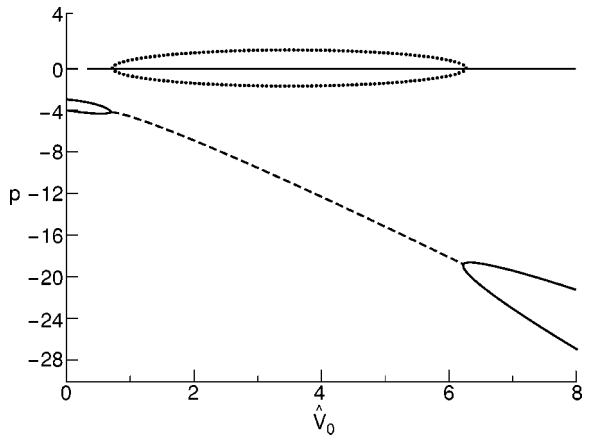

FIG. 5. The effect of poloidal $\sin\theta$-dependent flow, $\Delta_1'=-3.0$, $\Delta_2'=-4.0$. (i) Solid line, real eigenvalue p. (ii) Broken line, Re(p). (iii) Dotted line, Im(p).

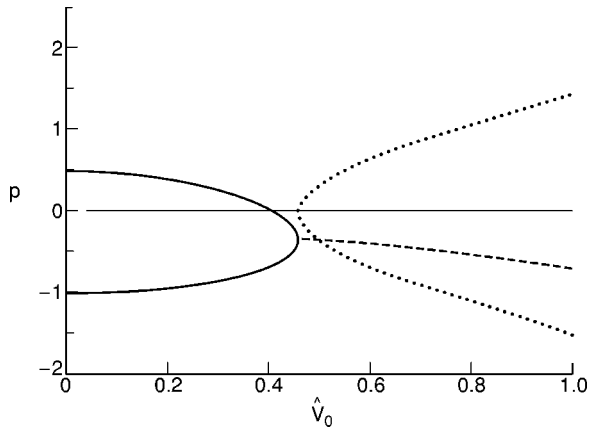

FIG. 7. The effect of poloidal $\sin\theta$-dependent flow, $\Delta_1'=-1.0$, $\Delta_2'=0.5$. (i) Solid line, real eigenvalue p. (ii) Broken line, Re(p). (iii) Dotted line, Im(p).

eigenvalues develop as $\hat{V}_0$ increases. They may remain real for all $\hat{V}_0$, tending asymptotically to $-2m\hat{V}_0$, or two eigenvalues may coalesce and give rise to a pair of stable complex eigenvalues. In Fig. 4 ($\Delta_1'=-1,\Delta_2'=-4$) the uppermost eigenvalue emanating from $p=-1$ at $\hat{V}_0=0$ remains real for all $\hat{V}_0$ whereas the next eigenvalue, emanating from $p=-4$, coalesces with a third eigenvalue and gives rise to a pair of stable, complex eigenvalues. In Fig. 5 ($\Delta_1'=-3,\Delta_2'=-4$) two stable eigenvalues also coalesce and give rise to a complex pair, but later these revert to two real eigenvalues and asymptotically approach $-2m\hat{V}_0$.

(b) In regions C ($\Delta_1'<0,\Delta_2'>0$) and E ($\Delta_1'>0,\Delta_2'<0$) there is one unstable and one stable eigenvalue at $\hat{V}_0=0$ and two typical ways for these eigenvalues to behave as $\hat{V}_0$ increases. In Fig. 6 ($\Delta_1'=-0.1,\Delta_2'=0.5$) the stable eigenvalue is first driven *unstable* as $\hat{V}_0$ increases. Subsequently it coalesces with the other unstable eigenvalue to give rise to unstable complex eigenvalues. These are eventually stabilized as the velocity increases further. Clearly the point $p=0$ at $\hat{V}_0\simeq 0.2$ does not define the stability boundary in this case. In Fig. 7 ($\Delta_1'=-1.0,\Delta_2'=0.5$) the unstable eigenvalue is first stabilized at $\hat{V}_0\simeq 0.4$ and only at higher $\hat{V}_0$ do the eigenvalues coalesce and give rise to stable complex eigenvalues. In this case $p=0$ *does* define the marginal stability boundary.

(c) In regions A_1 and A_2 there are two unstable eigenvalues at $\hat{V}_0=0$ and their typical behavior is illustrated in Fig. 8 ($\Delta_1'=2.0,\Delta_2'=0.5$). In this case the unstable eigenvalues first coalesce as $\hat{V}_0$ increases and give rise to unstable complex eigenvalues. These are subsequently stabilized as $\hat{V}_0$ increases beyond $\simeq 1.8$. There is no point $p=0$, in accord with the analysis of Sec. III C.

(d) In region B there are again two unstable eigenvalues at $\hat{V}_0=0$, and two typical ways in which they develop. In Fig. 9 ($\Delta_1'=4.2,\Delta_2'=0.5$) the lower eigenvalue is first stabilized at $\hat{V}_0\simeq 1.2$, but then goes *unstable* again as $\hat{V}_0$ increases further! It then coalesces with the higher eigenvalue to give unstable complex eigenvalues that eventually stabilize at a still higher velocity. There are two points $p=0$, in accord with the analysis of Sec. III C, but neither defines the marginal stability boundary. In Fig. 10 ($\Delta_1'=5.0,\Delta_2'=0.5$) both eigenvalues are

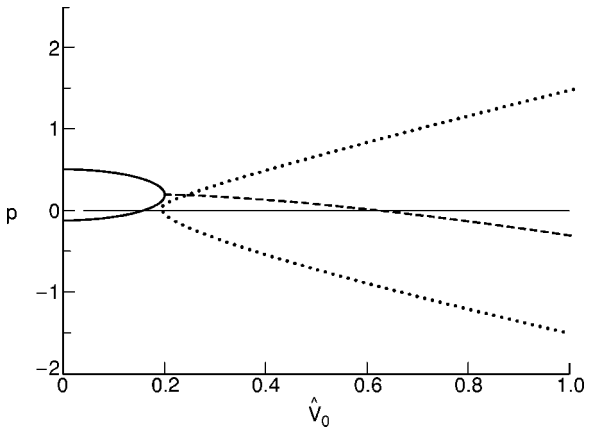

FIG. 6. The effect of poloidal $\sin\theta$-dependent flow, $\Delta_1'=-0.1$, $\Delta_2'=0.5$. (i) Solid line, real eigenvalue p. (ii) Broken line, Re(p). (iii) Dotted line, Im(p).

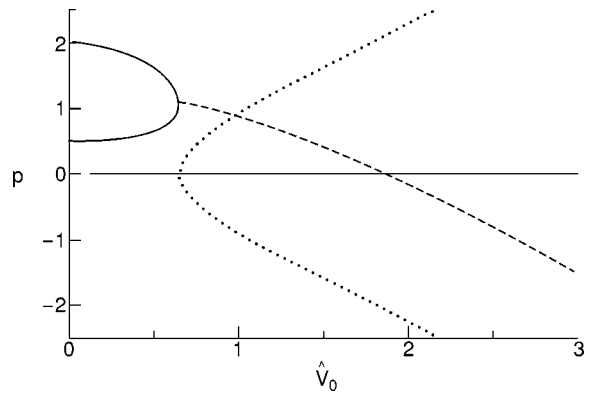

FIG. 8. The effect of poloidal $\sin\theta$-dependent flow, $\Delta_1'=2.0$, $\Delta_2'=0.5$. (i) Solid line, real eigenvalue p. (ii) Broken line, Re(p). (iii) Dotted line, Im(p).

Downloaded 08 Aug 2012 to 194.81.223.66. Redistribution subject to AIP license or copyright; see http://pop.aip.org/about/rights_and_permissions

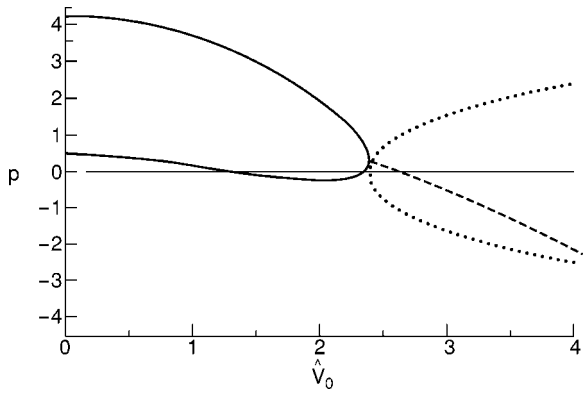

FIG. 9. The effect of poloidal sin θ dependent flow, $\Delta_1'=4.2$, $\Delta_2'=0.5$. (i) Solid line, real eigenvalue p. (ii) Broken line, Re(p). (iii) Dotted line, Im(p).

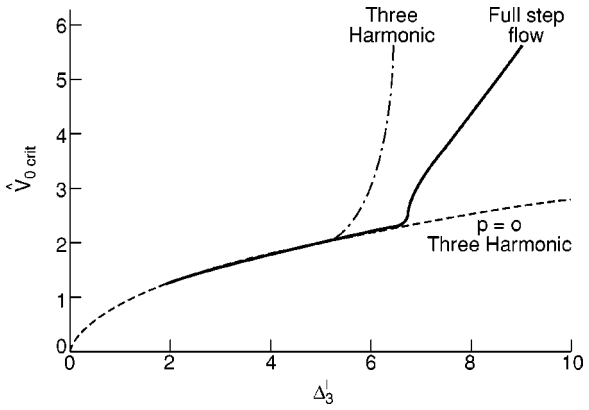

FIG. 11. Critical velocity needed to stabilize the nonresonant RWM (poloidal "step" flow).

stabilized before they coalesce to give complex eigenvalues. In this case the higher point $p=0$ *does* define the marginal stability boundary.

It is clear from these examples that with nonuniform poloidal wall rotation the behavior of RWMs is complicated—though they are always stabilized at a sufficiently high velocity. Modes with complex p frequently arise, but they are not associated with simple wall-locking, as was the case with toroidal rotation.

E. Step flow

The work so far described concerns the effect of wall rotation with sinusoidal variation in velocity. We have also carried out a limited investigation of a "step flow" variation of poloidal velocity, $V=V_0\,\mathrm{sign}(\theta)$, such as might represent a simple form of a flowing lithium wall blanket.

As noted earlier, for a step flow variation of velocity all Fourier harmonics b_m are directly coupled. In particular, the positive and negative m numbers are not decoupled as they are for sinusoidal variation. The effect of this coupling between distant Fourier modes can be seen in Fig. 11. This shows the critical velocity required for stability as a function of Δ_3' when all other Δ_m' are fixed. [In Fig. 11, $\Delta_0'=-2$, $\Delta_{\pm1}'=-2q_a/(q_a\mp1)$, $q_a=3$ and all other $\Delta_m'=-2|m|$.] The solid line shows the critical velocity with step flow variation, calculated retaining all Fourier harmonics $-40<m<40$. The broken line shows a similar calculation when only three harmonics $m=2,3,4$ are retained, as in Ref. 6. This "three-harmonic" approximation leads to a cubic equation for the eigenvalue p as a function of Δ_3':

$$F(p)=p^3+(12-\Delta_3')p^2+(32-12\Delta_3'+18\hat{V}_0^2)p+(96\hat{V}_0^2-32\Delta_3')=0. \tag{69}$$

By mapping the half plane $\mathrm{Re}(p)<0$ on to the complex F plane it can be shown that solutions of Eq. (69) correspond to stable modes provided

$$\hat{V}_0^2>\Delta_3'/3 \tag{70}$$

and

$$\hat{V}_0^2>\frac{2((\Delta_3')^2-12\Delta_3'+32)}{3\Delta_3'-20}, \tag{71}$$

so the larger of Eq. (70) and Eq. (71) defines the critical velocity. [Only when the critical velocity is given by Eq. (70) does it also correspond to $p=0$.]

It is interesting that in Fig. 11 the "three harmonic" approximation agrees well with the full calculation when $\Delta_3'\lesssim5$, but differs markedly for larger Δ_3'. Indeed in the three harmonic approximation the critical velocity $\to\infty$ as $\Delta_3'\to20/3$ whereas the full calculation remains finite. Another interesting feature is that the point at which the critical velocity ceases to be given by $p=0$ in the full step flow calculation is also at $\Delta_3'\simeq20/3$.

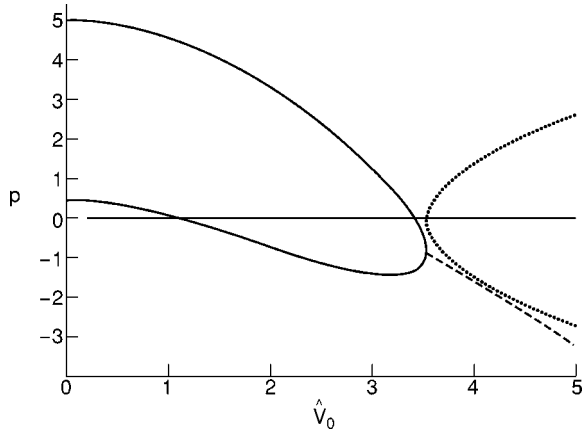

FIG. 10. The effect of poloidal sin θ-dependent flow, $\Delta_1'=5.0$, $\Delta_2'=0.5$. (i) Solid line, real eigenvalue p. (ii) Broken line, Re(p). (iii) Dotted line, Im(p).

IV. SUMMARY AND CONCLUSIONS

It is well known that Resistive Wall Modes are influenced by rotation of the wall relative to the plasma—because the skin effect makes the wall appear as an ideally conducting boundary. However, this effect disappears for perturbations that lock to the wall rather than to the plasma.[3] In this work we have examined the effect of *nonuniform* wall rota-

Downloaded 08 Aug 2012 to 194.81.223.66. Redistribution subject to AIP license or copyright; see http://pop.aip.org/about/rights_and_permissions

tion on RWMs in a torus. Nonuniform rotation should inhibit locking to the wall and may therefore provide stabilization of RWMs.

For a poloidally varying rotation, in either the toroidal or poloidal directions, the growth of RWMs is given as the eigenvalue p of a difference equation that depends only on the wall penetration time, τ_W, the wall velocity $V(\theta)$ and a set of indices Δ'_m. These indices depend on the plasma profile but are independent of wall rotation. Thus the problem is separated into two parts: (i) the determination of stability indices from the equilibrium profile and (ii) the determination of the effect of rotation when the indices are given. We have considered only problem (ii) here.

For a poloidally varying rotation in the toroidal direction we indeed find that rotation always reduces the growth rate of the most unstable mode below its zero velocity value. At high velocity, with a sinusoidal variation, we have shown analytically that RWMs tend to a universal damped nonresonant mode with $p \sim 2i\hat{V}_0 - \hat{V}_0^{1/3}$. This mode is peaked in poloidal angle and rotates toroidally at the maximum wall velocity $\hat{V}_0$. It is independent of the parameters Δ'_m, and therefore of the plasma profile. There may also be a damped resonant mode at high velocity that does not rotate. This is also universal in that it is independent of all Δ'_m except the resonant one. Its damping rate is determined, through the resonant Δ'_m, by the plasma response in the resonant layer—as explained in Sec. II D.

Numerically, for a set of tokamak-like indices Δ'_m, which correspond to a single $m=3$ unstable mode at $\hat{V}_0 = 0$, we find that this unstable mode does not rotate as the velocity increases: its growth rate diminishes and it is stabilized at $\hat{V}_0 \simeq 2.6$. Its damping rate then increases with $\hat{V}_0$ and at $\hat{V}_0 \sim 4.0$ it ceases to be the least stable mode. For $\hat{V}_0 \gtrsim 4$ the least stable mode is the complex frequency, wall locked, universal mode described above, with p asymptotic to $2i\hat{V}_0 - \hat{V}_0^{1/3}$ as $\hat{V}_0 \to \infty$.

For a set of parameters representing a system with an unstable resonant $m=2$ mode as well as an unstable nonresonant $m=3$ mode at $\hat{V}_0 = 0$, we find as $\hat{V}_0$ increases these two modes coalesce to form complex frequency modes which are stabilized at $\hat{V}_0 \simeq 2.8$. As in the previous numerical example, their damping then increases with $\hat{V}_0$ until at $\hat{V}_0 \simeq 4.0$ they also cease to be the least stable modes and are replaced by the universal resonant mode.

The case of nonuniform wall rotation in the poloidal direction differs considerably from that of toroidal rotation. The wall velocity is no longer constant along the direction of motion so an element of plasma experiences a varying, and indeed reversing, wall motion. Consequently wall locking is further inhibited and more complicated mode interactions occur.

For a sinusoidal variation of wall velocity there is an exact ''standard model'' solution for a particular set of Δ'_m ($\Delta'_m = -2|m|$ as is usual for large $|m|$). The model is atypical in that all RWMs are stable for any velocity, but it forms the basis for the study of more interesting situations. In particular, at large wall velocity the growth rate of RWMs tends to that of the standard model irrespective of the Δ'_m for small m and therefore (in most cases) independently of the plasma profile. Thus the standard model result $p_m = -2m\sqrt{1+\hat{V}_0^2}$ is universal for large poloidal rotation. However, the behavior of RWMs at intermediate velocities, between small rotation where $p_m \sim \Delta'_m$, and large rotation where $p_m \sim -2m\sqrt{1+\hat{V}_0^2}$, is complicated. This is indicated both analytically by an analysis of the $p=0$ situation and by numerical computation.

Considering the behavior of RWMs as a function of Δ'_1 and Δ'_2 with other Δ_m fixed, we found several regimes illustrated in Figs. 4–10. In the simplest situation the two modes corresponding to Δ'_1 and Δ'_2 at $\hat{V}_0 = 0$ are stabilized as $\hat{V}_0$ increases and the eigenvalues p_m are asymptotic to the universal values $-2m\sqrt{1+\hat{V}_0^2}$. However, in many cases these modes coalesce and give rise to complex frequency eigenvalues either before or after one or both modes are stabilized. For the parameter range examined ($-3 < \Delta'_1 < 5$, $-4 < \Delta'_2 < 0.5$) coalescence occurs in the region $0.2 \lesssim \hat{V}_0 \lesssim 3$. Eventually at sufficiently high velocity the eigenvalues must approach the standard values, though we have shown this numerically only in a few cases because of the difficulty in computing solutions for large $\hat{V}_0$.

In addition to the studies of the effect of sinusoidal variation in wall velocity we have carried out a limited examination of the effect on RWMs of a step variation $V_\theta = V_0 \,\mathrm{sign}(\theta)$ in wall velocity, such as might arise in the simplest form of a flowing lithium blanket. This step flow introduces additional long range coupling between poloidal Fourier modes. In a study of the critical velocity required for stability as a function of Δ'_3, with other Δ'_m fixed, we found that these additional couplings introduce little change when $\Delta'_3 < 5$. Indeed the results for $\Delta'_3 < 5$ were well reproduced by a simple model retaining only three harmonics. However, for $\Delta'_3 \gtrsim 5$ the computations with a full interaction between harmonics $-40 < m < 40$ differed dramatically from the three harmonic model (in which the critical velocity $\to \infty$ when $\Delta'_3 \to 20/3$).

ACKNOWLEDGMENTS

This work is jointly funded by UK DTI and EURATOM and by the U.S. Department of Energy.

APPENDIX: BEHAVIOR OF THE I_1, I_2, I_3 INTEGRALS AT LARGE FLOW

In this appendix we consider the large $\hat{V}_0$ behavior of the integrals I_1, I_2, I_3 required to determine the eigenvalue p when all Δ'_m have their standard values except for $m=l$. As we will see, the correction to the standard eigenvalue is small when $\hat{V}_0$ is large, so we may evaluate I_1, I_2, and I_3 at $p = -2m\sqrt{1+\hat{V}_0^2}$.

(i) The integral I_1,

$$I_1 = \oint d\theta F(\theta) e^{il\theta}, \tag{A1}$$

Downloaded 08 Aug 2012 to 194.81.223.66. Redistribution subject to AIP license or copyright; see http://pop.aip.org/about/rights_and_permissions

where

$$F=\exp\left[-(p/2)\int_0^\theta d\theta/r(\theta)\right]$$
$$=\left[\frac{(\hat{V}_0+\sqrt{1+\hat{V}_0^2})}{(\hat{V}_0-\sqrt{1-\hat{V}_0^2})}\frac{\tan\theta/2-i(\hat{V}_0-\sqrt{1+\hat{V}_0^2})}{\tan\theta/2-i(\hat{V}_0+\sqrt{1+\hat{V}_0^2})}\right]^m. \tag{A2}$$

For large $\hat{V}_0$, introducing $t=\tan\theta/2$, we can write I_1 as

$$I_1=-2(2\hat{V}_0)^{2m}\int_{-\infty}^{\infty}\left(\frac{t+i/2\hat{V}_0}{t-2i\hat{V}_0}\right)^m\frac{(t-i)^{l-1}}{(t+i)^{l+1}}dt. \tag{A3}$$

This can be evaluated conveniently by contour integration around the lower half t-plane. For large $\hat{V}_0$ the residue at the singularity $t=-i$ shows that

$$I_1\sim\hat{V}_0^m. \tag{A4}$$

(ii) The integral I_2,

$$I_2=\frac{1}{2\pi}\oint\frac{d\theta e^{-il\theta}}{r(\theta)F(\theta)}. \tag{A5}$$

We first integrate by parts to obtain

$$I_2=\frac{-i}{2\pi\sqrt{1+\hat{V}_0^2}}\oint\frac{d\theta e^{-il\theta}}{F(\theta)}. \tag{A6}$$

Introducing $t=\tan\theta/2$ as before, and at large $\hat{V}_0$,

$$I_2=-\frac{i}{\pi m\hat{V}_0}(2\hat{V}_0)^{2m}\int_{-\infty}^{\infty}\left(\frac{t-2i\hat{V}_0}{t+i/2\hat{V}_0}\right)^m\frac{(t+i)^{l-1}}{(t-i)^{l+1}}dt. \tag{A7}$$

This can be evaluated most conveniently by contour integration around the upper half t-plane. For large $\hat{V}_0$ the residue at $t=i$ shows that

$$I_2\sim\hat{V}_0^{-(m+1)}. \tag{A8}$$

Finally, for I_3,

$$I_3=\frac{1}{2\pi}\oint\frac{1}{r(\theta)}\exp\left(\frac{p}{2}R(\theta)-il\theta\right)$$
$$\times d\theta\int_{-\pi}^{\theta}\exp\left(-\frac{p}{2}R(\theta')+il\theta'\right)d\theta', \tag{A9}$$

we first integrate by parts to give

$$I_3=-\frac{1}{m\hat{V}_0}+\frac{I_1}{2\pi m\hat{V}_0}$$
$$+\frac{i}{2\pi m\hat{V}_0}\oint\frac{d\theta e^{-il\theta}}{F(\theta)}\int_{-\pi}^{\theta}e^{il\theta'}F(\theta')d\theta'. \tag{A10}$$

Thus I_3 is dominated by the term involving I_1 so that the result (A4) implies

$$I_3\sim\hat{V}_0^{m-1}. \tag{A11}$$

Then from Eq. (59) we find that the shift in the eigenvalue from its standard value is

$$\frac{\Delta p}{p}\sim\frac{1}{\hat{V}_0^m}, \tag{A12}$$

and therefore $\to 0$ as $\hat{V}_0\to\infty$.

[1] B. Alper, M. K. Bevir, H. A. B. Bodin *et al.*, Plasma Phys. Controlled Fusion **31**, 205 (1989).
[2] A. M. Garofalo, E. J. Strait, J. M. Bialek *et al.*, Nucl. Fusion **40**, 1491 (2000).
[3] C. G. Gimblett, Nucl. Fusion **26**, 617 (1986).
[4] C. G. Gimblett, Plasma Phys. Controlled Fusion **31**, 2183 (1989).
[5] T. H. Jensen and R Fitzpatrick, Phys. Plasmas **3**, 2641 (1996).
[6] L. Zakharov, "Stabilization of tokamak plasmas by lithium streams," submitted to Comments Plasma Phys. Control. Fusion.
[7] J. W. Connor, C. G. Gimblett, H. R. Wilson, J. P. Freidberg, and R. J. Hastie, *Theory of Fusion Plasmas* (Editrice Compositori, Bologna, 2000), p. 307.
[8] J. M. Finn, Phys. Plasmas **2**, 3782 (1995).
[9] C. G. Gimblett and R. J. Hastie, Phys. Plasmas **7**, 258 (2000).
[10] A. Bondeson and H. X. Xie, Phys. Plasmas **4**, 2081 (1997).
[11] R. Fitzpatrick, Nucl. Fusion **33**, 1049 (1993).

Downloaded 08 Aug 2012 to 194.81.223.66. Redistribution subject to AIP license or copyright; see http://pop.aip.org/about/rights_and_permissions